THE JOURNAL OF PHYSICAL CHEMISTRY LETTERS
A JOURNAL OF THE AMERICAN CHEMICAL SOCIETY

pubs.acs.org/JPCL

Letter

From Milliseconds to Minutes: Melittin Self-Assembly from Concerted Non-Equilibrium Pressure-Jump and Equilibrium Relaxation Nuclear Magnetic Resonance

Martin D. Gelenter, Wai-Ming Yau, Philip A. Anfinrud, and Ad Bax*

Cite This: *J. Phys. Chem. Lett.* 2024, 15, 1930−1935

Read Online

ACCESS | Metrics & More | Article Recommendations | Supporting Information

ABSTRACT: Non-equilibrium kinetics techniques like pressure-jump nuclear magnetic resonance (NMR) are powerful in tracking changes in oligomeric populations and are not limited by relaxation rates for the time scales of exchange that can be probed. However, these techniques are less sensitive to minor, transient populations than are Carr−Purcell−Meiboom−Gill (CPMG) relaxation dispersion experiments. We integrated non-equilibrium pressure-jump and equilibrium CPMG relaxation dispersion data to fully map the kinetic landscape of melittin tetramerization. While monomeric peptides weakly form dimers ($K_{d,D/M} \approx 26$ mM) whose population never exceeds 1.6% at 288 K, dimers associate tightly to form stable tetrameric species ($K_{d,T/D} \approx 740$ nM). Exchange between the monomer and dimer, along with exchange between the dimer and tetramer, occurs on the millisecond time scale. The NMR approach developed herein can be readily applied to studying the folding and misfolding of a wide range of oligomeric assemblies.

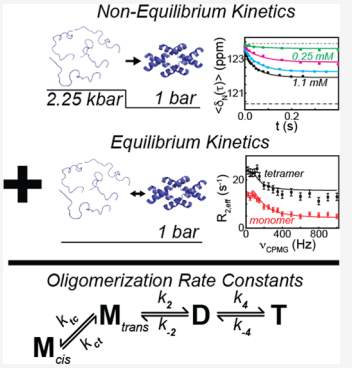

Protein folding, misfolding, and oligomerization are intrinsically tied to protein function and dysfunction.[1] The folding and assembly of homo-oligomeric proteins often control their activity and the rate at which they accomplish their function,[2] while misfolding and aggregation are implicated in many neurodegenerative diseases, including Alzheimer's, Parkinson's and Huntington's diseases.[3] The functional roles of proteins, in addition to pathologies, are often controlled by lowly populated, transient species that are difficult to characterize with traditional techniques such as fluorescence microscopy and light scattering.[4]

Equilibrium exchange nuclear magnetic resonance (NMR) techniques, such as Carr−Purcell−Meiboom−Gill relaxation dispersion (CPMG-RD),[5] $R_{1\rho}$ relaxation dispersion,[6] ^{15}N ZZ-exchange spectroscopy,[7,8] and chemical exchange saturation transfer (CEST),[9,10] have been widely used to detect lowly populated and transient species. Although these techniques are powerful in characterizing such species that are "invisible" to other techniques, they suffer from certain limitations that hinder the analysis of multiple states in exchange across time scales of many orders of magnitude, a situation that is often important for studying the functional and pathogenic roles of proteins. The time scales accessible to equilibrium exchange NMR experiments are determined by spin relaxation rates. CPMG-RD and R_{1r} relaxation dispersion experiments are limited by R_2 and R_{1r}, respectively, while ZZ-exchange spectroscopy and CEST are limited by the longitudinal relaxation rate, R_1, of the species being studied. In solution, R_1 values of interest are rarely $\lesssim 1$ s^{-1}, thus setting an upper limit of ∼1 s for exchange time scales that can be probed with equilibrium exchange NMR. However, many protein folding and aggregation processes have steps that occur on a time scale of seconds to minutes and are therefore impossible to study with equilibrium exchange NMR. Proline *cis*−*trans* isomerization is one example of a common rate-limiting step for protein folding processes and occurs on the minute time scale, making it inaccessible to equilibrium exchange NMR.[11]

Non-equilibrium techniques for studying protein folding and oligomerization, such as pressure-jump solution NMR spectroscopy[12−14] and inverse temperature jump followed by rapid freeze-quench solid-state NMR spectroscopy,[15] are especially useful in tracking large-scale population changes. In contrast to that of equilibrium exchange NMR, the time scales that can be probed with such techniques can be arbitrarily long. In this Letter, we harness the power and benefits of combined non-equilibrium and equilibrium techniques to define the pathway and the relevant exchange rates for the tetramerization of melittin, including the presence of a highly transient dimeric intermediate species.

Melittin, the active component of honeybee venom, is a 26-residue peptide containing a post-translational C-terminal amidation (section II of the Supporting Information) that

Received: December 20, 2023
Revised: January 25, 2024
Accepted: January 29, 2024
Published: February 12, 2024

https://doi.org/10.1021/acs.jpclett.3c03563
J. Phys. Chem. Lett. 2024, 15, 1930−1935

undergoes exchange between an intrinsically disordered monomer and an α-helical tetramer at millimolar peptide concentrations. Residual dipolar couplings (RDCs) measured in solution showed the same helical structure for the tetramer as observed via X-ray crystallography and predicted by AlphaFold-Multimer.[16] The melittin tetramer forms on the millisecond time scale from monomers with residue P14 in the *trans* conformation, while there is also a much slower off-pathway exchange between disordered monomers with P14 in the *trans* and *cis* conformations. Bioinformatics and mutation studies showed that P14 is required for efficient membranelytic activity,[17,18] but its isomerization appears to be unproductive, even though important for understanding the full kinetic pathway of melittin tetramerization. Proline *cis*–*trans* isomerization is rate-limiting and occurs on a time scale that is too slow to study with exchange-based equilibrium NMR techniques.

The population of melittin with P14 in the *cis* conformation is considerably larger when the peptide is pressure-denatured compared to atmospheric pressure, where at 1 mM approximately half of the peptide is in the all-*trans* tetrameric state (Figure 1a,b). To measure the kinetics of P14 *cis*–*trans*

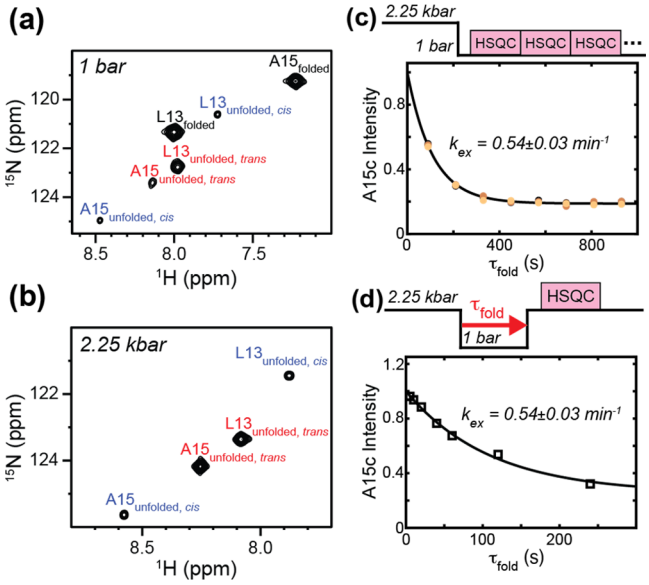

Figure 1. P14 *cis*–*trans* isomerization. ^{15}N–^{1}H HSQC spectra measured at 600 MHz and 288 K of synthetic melittin, enriched with ^{15}N at L13 and A15, at (a) atmospheric pressure and (b) 2.25 kbar, both at 1 mM. At atmospheric pressure, the folded, α-helical P14-*trans* tetramer, random coil P14-*trans* monomer, and random coil P14-*cis* monomer populations are in slow exchange equilibrium and resonances from each species are visible in the ^{15}N–^{1}H HSQC spectrum. At 2.25 kbar, melittin is pressure-denatured and the tetramer signals are no longer visible.[19] (c and d) P14 *cis*–*trans* isomerization kinetics for a 2.0 mM melittin sample probed via a single pressure jump and a double pressure jump, respectively. One k_{ex} value was globally fit for the data from both experiments.

isomerization (section IV of the Supporting Information), the sample was first pressure-denatured and equilibrated at 2.25 kbar and 288 K, where the unfolded monomer with P14 in the *cis* conformation, M_{cis}, makes up 11% of the total peptide concentration. Following a drop to atmospheric pressure, a series of short ^{15}N–^{1}H HSQC measurements were carried out, each 2 min in length, to track the decay of peaks arising from the M_{cis} population as the sample relaxed to its new equilibrium state at low pressure (Figure 1c).[20] This strategy worked well at low temperatures, such as 278 K, when the rate of P14 *cis*–*trans* isomerization was significantly slower than the duration of each HSQC (Figure S1).

At 288 K, P14 *cis*–*trans* isomerization occurs on a time scale that is comparable to the duration of an individual HSQC measurement, thereby limiting the temporal resolution (Figure 1c and Figure S2a,b). We therefore also carried out a double-jump experiment in which the pressure was dropped to atmospheric pressure for a variable time, τ_{fold}, before being jumped back to 2.25 kbar for a single-scan high-pressure readout HSQC (Figure 1d and Figure S2c,d). Although some fraction of the peptide reverts to the high-pressure equilibrium M_{cis} state during the readout HSQC, this percentage is always the same and simply results in an offset for the apparent M_{cis} concentration at equilibrium. The τ_{fold} delay therefore can be made arbitrarily short (within the limits of the pressure-jump apparatus hardware), enabling the probing of proline *cis*–*trans* isomerization with an arbitrary time resolution (Figure 1d). With a M_{cis} population of 11% and a k_{ex} of 0.54 ± 0.03 min^{-1}, the *cis* → *trans* (k_{ct}) and *trans* → *cis* (k_{tc}) rates are 0.49 ± 0.03 and 0.060 ± 0.006 min^{-1}, respectively.

To set bounds on the population and chemical shifts of the dimer, ^{15}N–^{1}H HSQCs at concentrations ranging from 0.05 to 2 mM were collected (Figure S3 and section III of the Supporting Information). Across this concentration range, the relative peak integrals, and thus populations, of the monomer and tetramer change dramatically, but no peaks corresponding to a dimer were observed. The dimer population, therefore, was either below the detection limit or in fast exchange with the monomer or tetramer populations. No chemical shift changes were observed for tetramer resonances, while some of the monomer peaks showed minute changes in chemical shift of at most a few hertz that were only slightly outside the measurement error (Figure S3). The dimer population therefore must be small and in fast exchange with the disordered monomer, while the tetramer must be in the slow exchange limit or have chemical shifts that are nearly identical to those of the dimer.

We then measured population-weighted average ^{15}N chemical shifts in a stroboscopic fashion using a double-jump pseudo-three-dimensional experiment with a high-pressure readout (Figure 2a, Figure S4, and section V of the Supporting Information).[21,22] For a given folding delay, τ_{fold}, this experiment gives a single, averaged ^{15}N chemical shift for each residue. If the "unfold and dissociate" period is sufficiently long to fully denature the protein and the stroboscopic chemical shift evolution period, κ, is much less than $\pi/\Delta\delta_N$, where $\Delta\delta_N$ is the chemical shift difference between the monomer and tetramer, then this average chemical shift represents a simple population-weighted average of the monomer, dimer, and tetramer populations. For several residues that fall outside this limit when κ = 1.25 ms, a comprehensive trigonometric analysis is necessary to accurately recapitulate the experimental data.[21] We utilized a 350 ms unfolding delay for all experiments, which results in an easily correctable 3% underestimate of the folded population due to an unfolding time constant of 100 ± 8 ms (Figure S5). At a concentration of 1.1 mM, the averaged chemical shifts cross the midpoint between the monomer and tetramer values at 123 ms (Figure 2b–e and Figure S6), corresponding to equal populations (Figure 3b). At lower concentrations, the

https://doi.org/10.1021/acs.jpclett.3c03563
J. Phys. Chem. Lett. 2024, 15, 1930–1935

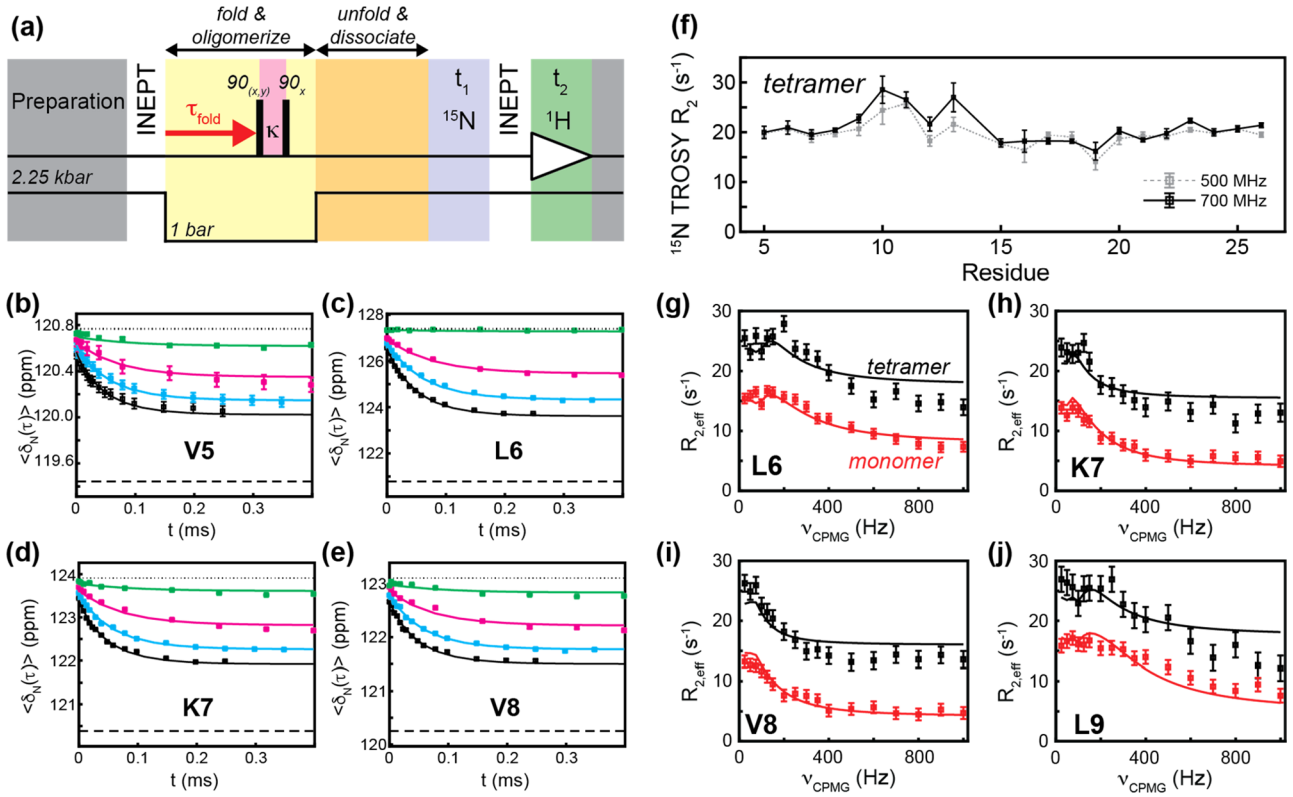

Figure 2. Non-equilibrium pressure-jump NMR and equilibrium CPMG-RD for studying oligomerization of uniformly $^{15}N/^{13}C/^{2}H$-enriched, C-terminally amidated melittin. (a) Schematic representation of the pseudo-three-dimensional pulse sequence used to measure population-weighted ^{15}N chemical shifts. While at high pressure, a refocused INEPT generates in-phase N_z magnetization prior to a pressure drop. After a delay, τ_{fold}, the population-weighted average ^{15}N chemical shift is encoded stroboscopically. The pressure is then jumped back to 2.25 kbar for a high-sensitivity $^{15}N-^{1}H$ HSQC readout in the unfolded state. (b–e) Time traces of the population-weighted average chemical shifts after a pressure drop to atmospheric pressure for V5, L6, K7, and V8, respectively, at 0.25 mM (green), 0.5 mM (magenta), 0.8 mM (light blue), and 1.1 mM (black). Solid lines show the best fit, simulated population-weighted average chemical shifts. The dashed and dotted black lines correspond to the chemical shifts of the tetramer and monomer, respectively. κ was set to 1.125 ms for the 0.25 mM sample and 0.5 ms for all other samples. (f) ^{15}N TROSY R_2 values for a 1.1 mM $^{2}H,^{13}C,^{15}N$-labeled melittin sample at 700 and 500 MHz ^{1}H frequencies. (g–j) ^{15}N in-phase CPMG relaxation dispersion curves for residues L6, K7, V8, and L9, respectively, in a 1.0 mM sample at 288 K on a 600 MHz spectrometer. Solid lines correspond to kinetic rate constants and equilibrium populations that were globally fit to both the pressure-jump and CPMG-RD data.

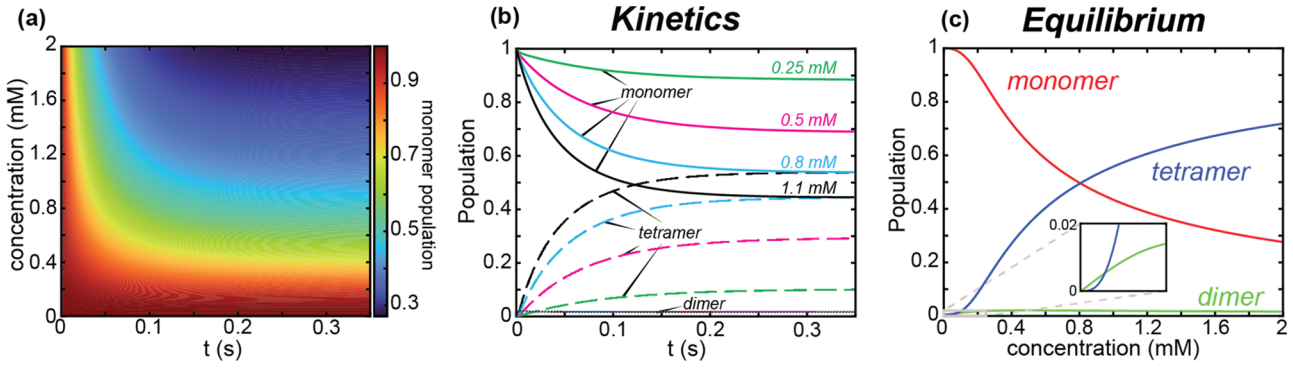

Figure 3. Kinetics and equilibrium of melittin oligomerization at 288 K. (a) Two-dimensional heat map depicting the loss of monomer over time for total peptide concentrations ranging from 0 to 2 mM. (b) Simulated kinetic profiles of the monomer, dimer, and tetramer populations for four concentrations studied by pressure-jump NMR. The dimer population never exceeds 1.6%. (c) Calculated monomer, dimer, and tetramer populations vs concentration at equilibrium.

equilibrium average shift is closer to the monomer, and the rate at which the average chemical shift changes is somewhat slower. The overall transition from the monomer to tetramer is well restrained by the pressure-jump data (Figure S7). However, considering that the data are well fit to a linear combination of the monomer and tetramer chemical shifts, the dimer and its chemical shifts are effectively invisible to these techniques; it is lowly populated and/or has chemical shifts that are close to those of the tetramer. Although AlphaFold-Multimer[23,24] predictions for the dimer had low model confidence scores (Figure S8c,d), all predicted dimer models had backbone torsion angles and thus predicted backbone

https://doi.org/10.1021/acs.jpclett.3c03563
J. Phys. Chem. Lett. 2024, 15, 1930−1935

chemical shifts[25] that were very similar to those of the tetramer (Figure S9).

We therefore turned to equilibrium exchange NMR, in the form of ^{15}N TROSY R_2[26] (section III of the Supporting Information) and ^{15}N CPMG-RD measurements (section VI of the Supporting Information) to restrain exchange parameters involving the dimer population.[27] ^{15}N TROSY R_2 measurements of a 1.0 mM sample showed nearly uniform R_2 values of ∼20 s^{-1} for the tetramer (Figure 2f). If the tetramer is in slow exchange with the dimer, its effective R_2 is controlled by the lifetime of the tetrameric species, i.e., the tetrameric dissociation rate constant, k_{-4}.[28] This sets an upper limit of 20 s^{-1} for k_{-4} and, assuming an average intrinsic ^{15}N TROSY R_2 of 6 s^{-1} for the 12 kDa homotetramer at 600 MHz, suggests that k_{-4} is ∼14 s^{-1}. Significant relaxation dispersion is observed in the CPMG-RD $R_{2,\mathrm{eff}}$ rates at CPMG frequencies ranging from 25 to 1000 Hz for the monomeric and tetrameric species (Figure 2g−j and Figure S10).[29]

To take advantage of both the pressure-jump data's tight restraints on the overall monomer to tetramer exchange along with the CPMG-RD restraints on M_{trans} to dimer and dimer to tetramer exchange, the non-equilibrium and equilibrium data were fit simultaneously to extract the dimer association and dissociation rate constants, k_2 and k_{-2}, respectively, along with the tetramer association and dissociation rate constants, k_4 and k_{-4}, respectively (section VIII of the Supporting Information). Data collected at four concentrations for the pressure-jump experiments and one concentration for the CPMG-RD measurements yielded convergence in the fit for all four rate constants and good agreement with the experimental data (Figure 2b−e,g−j). The kinetics and equilibrium partitioning are easily calculated for any range of concentrations (Figure 3a−c) by using the fitted rate constants (Scheme 1). As one

Scheme 1. Overall Kinetic Scheme for Melittin's Exchange among the Monomer, Dimer, and Tetramer at 288 K[a]

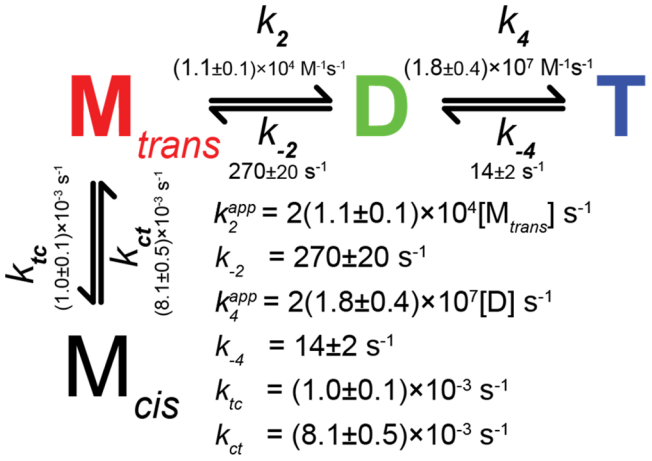

[a]Monomers with P14 in the *cis* conformation undergo exchange with the P14-*trans* at a rate that is 5 orders of magnitude slower than that of the M_{trans}−D−T exchange process.

can see from the fitted value ($K_{d,D/M}$ = 26 mM), the dimer is very unstable. The tetramer, on the contrary, shows a high affinity with a $K_{d,T/D}$ of 740 nM. Consequently, the dimer population never exceeds 1.6% of the total peptide, but the dimer nevertheless is the critical intermediate. The dimer is a highly transient species due to the relatively fast dimer dissociation and tetramer association. This result explains why the pressure-jump stroboscopic chemical shift measurements alone were not sufficient to restrain exchange parameters associated with the dimer. Although our CPMG-RD data also did not restrain the overall monomer to tetramer exchange (Figures S7 and S9),[29] these experiments are extremely sensitive to lowly populated states undergoing exchange on the millisecond time scale[30] and thus complement the pressure-jump data in terms of extracting kinetic rate constants involving lowly populated, transient species.

Molecular dynamics simulations have suggested that melittin forms partially disordered tetramers by sequential addition of monomers in <300 ns that later relax into a well-ordered crystal-like structure.[31,32] We see no evidence from chemical shifts, RDCs, or relaxation measurements for exchange between a rigid and partially disordered tetramer at early time points.[16] Furthermore, dimer−dimer addition has been observed to be ubiquitous in nature for homotetramer formation, possibly due to selective evolutionary pressure to avoid unwanted buildup of trimer species.[33] It is plausible that the increased temperature (310 K), a high peptide concentration (10 mM), and short time scales (<300 ns) studied in these simulations probed a qualitatively different tetramerization process to what we observed in solution at 288 K.

Previous experimental reports of melittin tetramerization kinetics in the literature used melittin concentrations and experimental conditions that make the monomer to dimer transition rate limiting and thus provided detailed kinetic rate constants for only this equilibrium, not the dimer to tetramer equilibrium.[15,34,35] With the buffer conditions used in our study, monomer to dimer exchange and dimer to tetramer exchange occur at the same rate for a total peptide concentration of 0.53 mM. At lower peptide concentrations, the dimer to tetramer transition is rate limiting, while at higher concentrations, the monomer to dimer exchange becomes rate limiting. We were therefore able to extract rate constants for both exchange processes because our pressure-jump data spanned concentrations ranging from 0.25 to 1.1 mM.

Herein, we combined the benefits of non-equilibrium pressure-jump NMR experiments with equilibrium relaxation measurements to map out the kinetic landscape of melittin's equilibrium between an intrinsically disordered monomer and an α-helical tetramer. Pressure-jump NMR kinetics experiments are particularly powerful in tracking the change in major populations across many time scales, while CPMG-RD is exquisitely sensitive to lowly populated, transient states. Furthermore, the high-pressure readout for the pressure-jump experiments makes these experiments readily amenable to studying systems whose resonances are severely line-broadened at atmospheric pressure due to exchange and the slow rotational correlation time of oligomeric assemblies.

Isomerization of P14 occurs on a time scale of minutes and is rate limiting for tetramerization, exemplifying a process that is inaccessible to traditional equilibrium kinetics techniques. Exchange between *trans*-P14 monomers and dimer, along with exchange between the dimer and tetramer, occurs on the millisecond time scale. While the pressure-jump NMR stroboscopic chemical shift measurements are sensitive to large population changes and thus the monomer to tetramer exchange, they are less sensitive to lowly populated states, to which CPMG-RD is especially sensitive. A global fit to both the non-equilibrium and equilibrium kinetics data provides a

https://doi.org/10.1021/acs.jpclett.3c03563
J. Phys. Chem. Lett. 2024, 15, 1930−1935

complete picture of this oligomerization process spanning a time scale of 5 orders of magnitude.

Our approach can readily be applied to study the folding and misfolding of a wide range of oligomeric proteins. For example, proteases, such as the HIV-1 protease, are active in only the dimeric state and unstable as folded monomers.[36] For such systems, pressure-jump and relaxation measurements can elucidate the kinetic and equilibrium landscapes of the folding and dimerization processes. Additionally, these methods can be applied to studying the initial molecular events associated with neurodegenerative diseases that involve oligomers either in the pathology or as a prenucleation step in a fibril aggregation process. For systems like Aβ_{40},[37] Aβ_{42},[38] Huntington,[39] and transthyretin,[40] these techniques may enhance the understanding of how the proteins misfold and form toxic aggregates, potentially a key step in developing therapies to slow or stop progression of such diseases.

■ ASSOCIATED CONTENT

Supporting Information

The Supporting Information is available free of charge at https://pubs.acs.org/doi/10.1021/acs.jpclett.3c03563.

Materials and Methods, including detailed descriptions of sample preparation, experimental parameters, and the associated data analysis; additional supplemental figures; and tables with chemical shifts and relaxation parameters used in the fitting of the non-equilibrium pressure-jump and equilibrium relaxation NMR data (PDF)

Transparent Peer Review report available (PDF)

■ AUTHOR INFORMATION

Corresponding Author

Ad Bax − *Laboratory of Chemical Physics, National Institute of Diabetes and Digestive and Kidney Diseases, National Institutes of Health, Bethesda, Maryland 20892, United States;* orcid.org/0000-0002-9809-5700; Email: bax@nih.gov

Authors

Martin D. Gelenter − *Laboratory of Chemical Physics, National Institute of Diabetes and Digestive and Kidney Diseases, National Institutes of Health, Bethesda, Maryland 20892, United States*

Wai-Ming Yau − *Laboratory of Chemical Physics, National Institute of Diabetes and Digestive and Kidney Diseases, National Institutes of Health, Bethesda, Maryland 20892, United States*

Philip A. Anfinrud − *Laboratory of Chemical Physics, National Institute of Diabetes and Digestive and Kidney Diseases, National Institutes of Health, Bethesda, Maryland 20892, United States*

Complete contact information is available at: https://pubs.acs.org/10.1021/acs.jpclett.3c03563

Notes

The authors declare no competing financial interest.

■ ACKNOWLEDGMENTS

The authors thank J. L. Baber, J. Ying, and Y. Shen for technical support; E. Masoumzadeh, T. Schmidt, V. Tugarinov, G. M. Clore, D. A. Torchia, J. Lopez, J. M. Louis, and R. Tycko for insightful discussions; and G. Abdoulaeva for peptide synthesis. This work was supported by the Intramural Research Program of the National Institutes of Diabetes and Digestive and Kidney Diseases (DK075141).

■ REFERENCES

(1) Colón, W.; Church, J.; Sen, J.; Thibeault, J.; Trasatti, H.; Xia, K. Biological Roles of Protein Kinetic Stability. *Biochemistry* **2017**, *56* (47), 6179−6186.

(2) Goyal, B.; Goyal, D. Targeting the Dimerization of the Main Protease of Coronaviruses: A Potential Broad-Spectrum Therapeutic Strategy. *ACS Comb. Sci.* **2020**, *22* (6), 297−305.

(3) Ross, C. A.; Poirier, M. A. Protein Aggregation and Neurodegenerative Disease. *Nat. Med.* **2004**, *10* (7), S10−S17.

(4) Alderson, T. R.; Kay, L. E. Unveiling Invisible Protein States with NMR Spectroscopy. *Curr. Opin. Struct. Biol.* **2020**, *60*, 39−49.

(5) Hansen, D. F.; Vallurupalli, P.; Kay, L. E. An Improved 15N Relaxation Dispersion Experiment for the Measurement of Millisecond Time-Scale Dynamics in Proteins. *J. Phys. Chem. B* **2008**, *112* (19), 5898−5904.

(6) Gu, S.; Szymanski, E. S.; Rangadurai, A. K.; Shi, H.; Liu, B.; Manghrani, A.; Al-Hashimi, H. M. Dynamic Basis for dA•dGTP and dA•d8OGTP Misincorporation via Hoogsteen Base Pairs. *Nat. Chem. Biol.* **2023**, *19* (7), 900−910.

(7) Zhang, Y.; Kitazawa, S.; Peran, I.; Stenzoski, N.; McCallum, S. A.; Raleigh, D. P.; Royer, C. A. High Pressure ZZ-Exchange NMR Reveals Key Features of Protein Folding Transition States. *J. Am. Chem. Soc.* **2016**, *138* (46), 15260−15266.

(8) Li, Y.; Palmer, A. G. TROSY-Selected ZZ-Exchange Experiment for Characterizing Slow Chemical Exchange in Large Proteins. *J. Biomol. NMR* **2009**, *45* (4), 357−360.

(9) Vallurupalli, P.; Bouvignies, G.; Kay, L. E. Studying "Invisible" Excited Protein States in Slow Exchange with a Major State Conformation. *J. Am. Chem. Soc.* **2012**, *134* (19), 8148−8161.

(10) Cabrera Allpas, R.; Hansen, A. L.; Brüschweiler, R. ARCHE-NOAH: NMR Supersequence with Five Different CEST Experiments for Studying Protein Conformational Dynamics. *Phys. Chem. Chem. Phys.* **2023**, *25* (24), 16217−16221.

(11) Wedemeyer, W. J.; Welker, E.; Scheraga, H. A. Proline Cis−Trans Isomerization and Protein Folding. *Biochemistry* **2002**, *41* (50), 14637−14644.

(12) Kremer, W.; Arnold, M.; Munte, C. E.; Hartl, R.; Erlach, M. B.; Koehler, J.; Meier, A.; Kalbitzer, H. R. Pulsed Pressure Perturbations, an Extra Dimension in NMR Spectroscopy of Proteins. *J. Am. Chem. Soc.* **2011**, *133* (34), 13646−13651.

(13) Roche, J.; Royer, C. A.; Roumestand, C. Monitoring Protein Folding through High Pressure NMR Spectroscopy. *Prog. Nucl. Magn. Reson. Spectrosc.* **2017**, *102*−*103*, 15−31.

(14) Charlier, C.; Alderson, T. R.; Courtney, J. M.; Ying, J.; Anfinrud, P.; Bax, A. Study of Protein Folding under Native Conditions by Rapidly Switching the Hydrostatic Pressure inside an NMR Sample Cell. *Proc. Natl. Acad. Sci. U. S. A.* **2018**, *115* (18), E4169−E4178.

(15) Wilson, C. B.; Tycko, R. Millisecond Time-Resolved Solid-State NMR Initiated by Rapid Inverse Temperature Jumps. *J. Am. Chem. Soc.* **2022**, *144* (22), 9920−9925.

(16) Gelenter, M. D.; Bax, A. Recombinant Expression and Chemical Amidation of Isotopically Labeled Native Melittin. *J. Am. Chem. Soc.* **2023**, *145* (7), 3850−3854.

(17) Rex, S. A Pro→Ala Substitution in Melittin Affects Self-Association, Membrane Binding and Pore-Formation Kinetics Due to Changes in Structural and Electrostatic Properties. *Biophys. Chem.* **2000**, *85* (2), 209−228.

(18) Krauson, A. J.; He, J.; Wimley, W. C. Gain-of-Function Analogues of the Pore-Forming Peptide Melittin Selected by Orthogonal High-Throughput Screening. *J. Am. Chem. Soc.* **2012**, *134* (30), 12732−12741.

(19) Thompson, R. B.; Lakowicz, J. R. Effect of Pressure on the Self-Association of Melittin. *Biochemistry* **1984**, *23* (15), 3411−3417.

(20) Hauer, H.; Lüdemann, H. D.; Jaenicke, R. Free Activation Energies and Activation Volumes for the Amide Rotation in Some Peptides Studied by High Pressure 1H-High Resolution NMR. *Z. Naturforsch. [C]* **1982**, *37* (1−2), 51−56.
(21) Charlier, C.; Courtney, J. M.; Alderson, T. R.; Anfinrud, P.; Bax, A. Monitoring 15N Chemical Shifts During Protein Folding by Pressure-Jump NMR. *J. Am. Chem. Soc.* **2018**, *140* (26), 8096−8099.
(22) Chiliveri, S. C.; Shen, Y.; Baber, J. L.; Ying, J.; Sagar, V.; Wistow, G.; Anfinrud, P.; Bax, A. Experimental NOE, Chemical Shift, and Proline Isomerization Data Provide Detailed Insights into Amelotin Oligomerization. *J. Am. Chem. Soc.* **2023**, *145* (32), 18063−18074.
(23) Jumper, J.; Evans, R.; Pritzel, A.; Green, T.; Figurnov, M.; Ronneberger, O.; Tunyasuvunakool, K.; Bates, R.; Žídek, A.; Potapenko, A.; Bridgland, A.; Meyer, C.; Kohl, S. A. A.; Ballard, A. J.; Cowie, A.; Romera-Paredes, B.; Nikolov, S.; Jain, R.; Adler, J.; Back, T.; Petersen, S.; Reiman, D.; Clancy, E.; Zielinski, M.; Steinegger, M.; Pacholska, M.; Berghammer, T.; Bodenstein, S.; Silver, D.; Vinyals, O.; Senior, A. W.; Kavukcuoglu, K.; Kohli, P.; Hassabis, D. Highly Accurate Protein Structure Prediction with AlphaFold. *Nature* **2021**, *596* (7873), 583−589.
(24) Evans, R.; O'Neill, M.; Pritzel, A.; Antropova, N.; Senior, A.; Green, T.; Žídek, A.; Bates, R.; Blackwell, S.; Yim, J.; Ronneberger, O.; Bodenstein, S.; Zielinski, M.; Bridgland, A.; Potapenko, A.; Cowie, A.; Tunyasuvunakool, K.; Jain, R.; Clancy, E.; Kohli, P.; Jumper, J.; Hassabis, D. Protein Complex Prediction with AlphaFold-Multimer. *bioRxiv* **2022**, DOI: 10.1101/2021.10.04.463034.
(25) Shen, Y.; Bax, A. SPARTA+: A Modest Improvement in Empirical NMR Chemical Shift Prediction by Means of an Artificial Neural Network. *J. Biomol. NMR* **2010**, *48* (1), 13−22.
(26) Wang, C.; Palmer III, A. G. Solution NMR Methods for Quantitative Identification of Chemical Exchange in 15N-Labeled Proteins. *Magn. Reson. Chem.* **2003**, *41* (10), 866−876.
(27) Kotler, S. A.; Tugarinov, V.; Schmidt, T.; Ceccon, A.; Libich, D. S.; Ghirlando, R.; Schwieters, C. D.; Clore, G. M. Probing Initial Transient Oligomerization Events Facilitating Huntingtin Fibril Nucleation at Atomic Resolution by Relaxation-Based NMR. *Proc. Natl. Acad. Sci. U. S. A.* **2019**, *116* (9), 3562−3571.
(28) Charlier, C.; Cousin, S. F.; Ferrage, F. Protein Dynamics from Nuclear Magnetic Relaxation. *Chem. Soc. Rev.* **2016**, *45* (9), 2410−2422.
(29) Rennella, E.; Sekhar, A.; Kay, L. E. Self-Assembly of Human Profilin-1 Detected by Carr-Purcell-Meiboom-Gill Nuclear Magnetic Resonance (CPMG NMR) Spectroscopy. *Biochemistry* **2017**, *56* (5), 692−703.
(30) Reid Alderson, T.; Adriaenssens, E.; Asselbergh, B.; Pritišanac, I.; Van Lent, J.; Gastall, H. Y.; Wälti, M. A.; Louis, J. M.; Timmerman, V.; Baldwin, A. J.; LP Benesch, J. A Weakened Interface in the P182L Variant of HSP27 Associated with Severe Charcot-Marie-Tooth Neuropathy Causes Aberrant Binding to Interacting Proteins. *EMBO J.* **2021**, *40* (8), No. e103811.
(31) Liao, C.; Esai Selvan, M.; Zhao, J.; Slimovitch, J. L.; Schneebeli, S. T.; Shelley, M.; Shelley, J. C.; Li, J. Melittin Aggregation in Aqueous Solutions: Insight from Molecular Dynamics Simulations. *J. Phys. Chem. B* **2015**, *119* (33), 10390−10398.
(32) Shelley, M. Y.; Selvan, M. E.; Zhao, J.; Babin, V.; Liao, C.; Li, J.; Shelley, J. C. A New Mixed All-Atom/Coarse-Grained Model: Application to Melittin Aggregation in Aqueous Solution. *J. Chem. Theory Comput.* **2017**, *13* (8), 3881−3897.
(33) Powers, E. T.; Powers, D. L. A Perspective on Mechanisms of Protein Tetramer Formation. *Biophys. J.* **2003**, *85* (6), 3587−3599.
(34) Schwarz, G.; Beschiaschvili, G. Kinetics of Melittin Self-Association in Aqueous Solution. *Biochemistry* **1988**, *27* (20), 7826−7831.
(35) Jeon, J.; Thurber, K. R.; Ghirlando, R.; Yau, W.-M.; Tycko, R. Application of Millisecond Time-Resolved Solid State NMR to the Kinetics and Mechanism of Melittin Self-Assembly. *Proc. Natl. Acad. Sci. U. S. A.* **2019**, *116* (34), 16717−16722.
(36) Hayashi, H.; Takamune, N.; Nirasawa, T.; Aoki, M.; Morishita, Y.; Das, D.; Koh, Y.; Ghosh, A. K.; Misumi, S.; Mitsuya, H. Dimerization of HIV-1 Protease Occurs through Two Steps Relating to the Mechanism of Protease Dimerization Inhibition by Darunavir. *Proc. Natl. Acad. Sci. U. S. A.* **2014**, *111* (33), 12234−12239.
(37) Barnes, C. A.; Robertson, A. J.; Louis, J. M.; Anfinrud, P.; Bax, A. Observation of β-Amyloid Peptide Oligomerization by Pressure-Jump NMR Spectroscopy. *J. Am. Chem. Soc.* **2019**, *141* (35), 13762−13766.
(38) Wälti, M. A.; Orts, J.; Vögeli, B.; Campioni, S.; Riek, R. Solution NMR Studies of Recombinant Aβ(1−42): From the Presence of a Micellar Entity to Residual β-Sheet Structure in the Soluble Species. *ChemBioChem.* **2015**, *16* (4), 659−669.
(39) Chen, M.; Wolynes, P. G. Aggregation Landscapes of Huntingtin Exon 1 Protein Fragments and the Critical Repeat Length for the Onset of Huntington's Disease. *Proc. Natl. Acad. Sci. U. S. A.* **2017**, *114* (17), 4406−4411.
(40) Sun, X.; Ferguson, J. A.; Dyson, H. J.; Wright, P. E. A Transthyretin Monomer Intermediate Undergoes Local Unfolding and Transient Interaction with Oligomers in a Kinetically Concerted Aggregation Pathway. *J. Biol. Chem.* **2022**, *298* (8), 102162.

https://doi.org/10.1021/acs.jpclett.3c03563
J. Phys. Chem. Lett. 2024, 15, 1930−1935